Charge-exchange-induced two-electron satellite transitions from autoionizing levels in dense plasmas

F. B. Rosmej,[1,*] H. R. Griem,[2] R. C. Elton,[2] V. L. Jacobs,[3] J. A. Cobble,[4] A. Ya. Faenov,[5] T. A. Pikuz,[5] M. Geißel,[1] D. H. H. Hoffmann,[1] W. Süß,[1] D. B. Uskov,[6] V. P. Shevelko,[6] and R. C. Mancini[7]

[1]*GSI-Darmstadt, Plasmaphysik, Planckstrasse 1, D-64291 Darmstadt, Germany*

[2]*Institute for Research in Electronics and Applied Physics, University of Maryland, College Park, Maryland 20742-3511*

[3]*Center for Computational Materials Science, Materials Science and Technology Division, Naval Research Laboratory, Washington, D.C. 20375-5345*

[4]*Los Alamos National Laboratory, Los Alamos, New Mexico 87545*

[5]*Multicharged Ions Spectra Data Center of VNIIFRI, Russian Committee of Standards, Mendeleevo, 141570 Moscow Region, Russia*

[6]*Lebedev Physical Institute, Moscow, Russia*

[7]*Department of Physics, University of Nevada, Reno, Nevada 89557-0058*

(Received 29 May 2002; published 11 November 2002)

Order-of-magnitude anomalously high intensities for two-electron (dielectronic) satellite transitions, originating from the He-like $2s^2\ ^1S_0$ and Li-like $1s2s^2\ ^2S_{1/2}$ autoionizing states of silicon, have been observed in dense laser-produced plasmas at different laboratories. Spatially resolved, high-resolution spectra and plasma images show that these effects are correlated with an intense emission of the He-like $1s3p\ ^1P-1s^2\ ^1S$ lines, as well as the K_α lines. A time-dependent, collisional-radiative model, allowing for non-Maxwellian electron-energy distributions, has been developed for the determination of the relevant nonequilibrium level populations of the silicon ions, and a detailed analysis of the experimental data has been carried out. Taking into account electron density and temperature variations, plasma optical-depth effects, and hot-electron distributions, the spectral simulations are found to be not in agreement with the observations. We propose that highly stripped target ions (e.g., bare nuclei or H-like $1s$ ground-state ions) are transported into the dense, cold plasma (predominantly consisting of *L*- and *M*-shell ions) near the target surface and undergo single- and double-electron charge-transfer processes. The spectral simulations indicate that, in dense and optically thick plasmas, these charge-transfer processes may lead to an enhancement of the intensities of the two-electron transitions by up to a factor of 10 relative to those of the other emission lines, in agreement with the spectral observations.

DOI: 10.1103/PhysRevE.66.056402 PACS number(s): 52.70.La, 32.70.Fw, 32.80.Dz, 34.70.+e

I. INTRODUCTION

Following the publication of the first monograph on plasma spectroscopy [1], spectroscopic methods have provided essential information about basic plasma parameters and relevant physical processes. The accessible parameter range covers orders of magnitude in temperature and (especially) density, because practically all elements of particular, selected isoelectronic sequences can be used for diagnostic investigations. These elements may occur as intrinsic impurities or may be intentionally injected in small amounts. Detailed reviews of spectroscopic methods have been published subsequently [2–4].

In addition to the traditionally used resonance lines, dielectronic satellite spectra, which arise from radiative transitions from autoionizing states, have been successfully exploited for diagnostic investigations [5]. With the development of high-intensity lasers and the associated investigation of laser-produced plasmas, dielectronic-satellite transitions have become of increasing importance for the fundamental understanding of atomic radiation processes in plasmas. The primary application of dielectronic-satellite spectra has been as a temperature diagnostic. In the low-density coronal-model approximation, the intensity ratio of the dielectronic-satellite transition following radiationless electron capture—and the corresponding resonance-line transition—is predicted to be a function of the electron temperature and independent of the electron density [5]. Density and opacity effects can become important only in high-density plasma environments.

In laser-produced plasmas, satellite features near the H-like Ly_α lines have been observed which could not be interpreted in terms of temperature variations alone. Consequently, these satellite features have been characterized as exhibiting anomalous satellite intensities. It has been predicted [6,7] that collisionally induced transitions among the autoionizing states can lead to significant modifications of the autoionizing-level populations in dense plasmas, resulting in corresponding density-dependent deviations from the coronal-model values of the satellite intensities. At low densities, the satellite intensities had been shown to be proportional to the satellite-intensity *Q* factor introduced by Gabriel [5] and defined as follows:

$$Q_{ij}=\frac{g_j\Gamma_{j,g}A_{ji}}{\sum_k A_{jk}+\sum_l \Gamma_{jl}}. \tag{1}$$

Here g_j is the statistical weight of the autoionizing level j, $\Gamma_{j,g}$ is the autoionizing rate for the transition from the level j to the ground level g of the residual ion, and A_{ji} is the

*Electronic mail: rosmej@yahoo.de

radiative-emission rate for the satellite transition $j \rightarrow i$. The summations over k and l are to be taken over all permissible channels for radiative decay and autoionization, respectively. Detailed calculations, for the relevant atomic structure together with the collisional- and radiative-transition parameters, have been employed in investigations of electron-density effects for the Li-like satellite transitions $1s2\ell2\ell' \rightarrow 1s^2 2\ell + h\nu$ [7], which occur near the He_α $1s2p\ ^1P_1 \rightarrow 1s^2\ ^1S_0 + h\nu$ line, and for the $1s2\ell3\ell' \rightarrow 1s^2 2\ell + h\nu$ satellite transitions [8], which occur near the He_β $1s3p\ ^1P_1 \rightarrow 1s^2\ ^1S_0 + h\nu$ line. The Li-like $1s2\ell3\ell'$ satellite features offer the advantage that their intensities are particularly sensitive to electron-density variations near the critical density for typical laser experiments (e.g., $\lambda = 1\ \mu$m, Al target [9]).

The development of high-resolution, high-quality optical instruments, e.g., spherically bent mica crystals [10], has led to the demonstration that the satellite transitions can play a significant role in the emission of line radiation in high-intensity laser-produced plasmas. For plasmas near the target surface, the analysis of satellite transitions has been demonstrated to be an indispensable method for the interpretation of line-emission spectra. Under certain conditions, the satellite intensities may exceed the intensity of the corresponding (opacity-broadened) resonance lines [11,12].

The present investigation has been devoted to the analysis of dielectronic satellite lines arising from particular two-electron transitions. Specifically, we have considered the He-like satellite lines $O = 2s^2\ ^1S_0 \rightarrow 1s2p\ ^1P_1 + h\nu$ and $P = 2s^2\ ^1S_0 \rightarrow 1s2p\ ^3P_1 + h\nu$ (which occur near the Ly_α line) and the Li-like satellite lines $o = 1s2s^2\ ^2S_{1/2} \rightarrow 1s^2 2p\ ^2P_{3/2} + h\nu$ and $p = 1s2s^2\ ^2S_{1/2} \rightarrow 1s^2 2p\ ^2P_{1/2} + h\nu$ (which occur near the He_α line). These particular satellite lines, which are located on the far-red side of the majority of the $2\ell2\ell'$ and $1s2\ell2\ell'$ satellite lines, had been neglected in previous interpretations of soft x-ray spectra. However, in recent experiments [13] performed at the LANL TRIDENT laser facility, these satellite features were observed with unusually high intensities.

We have performed an extensive investigation of these satellite features at the nhelix laser facility at GSI-Darmstadt. This investigation has included the application of high-resolution x-ray spectromicroscopy and the utilization of various calculations for the relevant atomic structure, radiative transition rates, and collision cross sections. Finally, we have introduced a new collisional-radiative model for the spectral analysis of the satellite transitions, in which account is taken of the populations of the autoionizing states due to charge-transfer processes between ions of various charge stages in penetrating plasmas. We show that this additional population mechanism can account for the recent spectral observations.

II. EXPERIMENTAL ARRANGEMENTS, X-RAY SPECTRA, AND PLASMA IMAGES

The TRIDENT facility at the Los Alamos National Laboratory features a Nd-glass laser, which is operated with an energy of 170 J in each of two beams and a pulse width of 1 ns (nearly a Gaussian shape). With a focal spot size of 500 μm, an intensity of 9×10^{13} W/cm^2 was focused onto planar targets. These targets where illuminated at 30° to the normal from both sides. These experiments [13] were performed using a frequency-doubled laser wavelength of $\lambda = 0.53\ \mu$m and 20-μm thin silicon targets. The spectra were dispersed with a KAP crystal and viewed along an axis tangential to the target surface. Detection was achieved with a 90-ps-gated, four-strip microchannel plate, which was tested for linearity with respect to the intensity. A slit for each stripline provided spatial resolution of a few micrometers normal to the target surface. The spectral data were then recorded with a charge-coupled-device (CCD) camera. An electron temperature as high as $kT_e = 800 \pm 200$ eV was deduced from Thomson-scattering measurements, extending to a distance of a few hundred micrometers from the target surface with about 110 ps time resolution. This electron temperature is consistent with the values used in our present spectral modeling. Figure 1, which is traced close to the target surface, shows an experimental silicon spectrum covering the wavelength region from the He_β line to the K_α line. Relatively intense emissions were observed to be produced by the He-like (O, P) and Li-like (o, p) dielectronic-satellite transitions, originating from the upper autoionizing states $2s^2$ and $1s2s^2$, respectively. Intense K_α and He_β lines were also observed. We emphasize that these observations were found to be uniquely associated with emissions that were produced very close to the target surface [13].

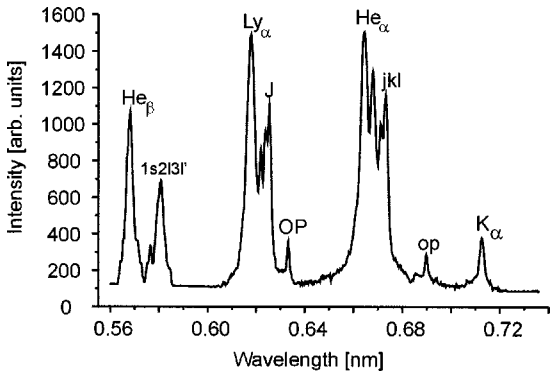

FIG. 1. Silicon-emission spectrum observed close to the target surface at the TRIDENT laser facility. The Li-like *op*-satellite emissions and the He-like *OP*-satellite emissions are unusually intense compared with the emissions in the *jkl*- and *J*-satellite transitions, respectively.

The nhelix laser is a Nd-glass/YAG laser, with $\lambda = 1.064\ \mu$m, an energy of 20 J, and a pulse width of 15 ns (nearly a Gaussian shape). With a focal spot size of about 300 μm, an intensity of about 10^{12} W/cm^2 is produced normal to massive (and thin-foil) Mg-slab targets. The novel spectroscopic diagnostics simultaneously employs several spherically bent mica crystals, providing spectral and spatial resolution in different orientations (parallel and perpendicular to the target surface). The spectral resolving power achieved is $\lambda/\delta\lambda \approx 4000$, and the spatial resolution is 20 μm. Spectra were recorded with Kodak DEF-5 film and analyzed with a 10 000–dpi drum scanner. The time-integrated spectra have been corrected for filter transmission [14], film re-

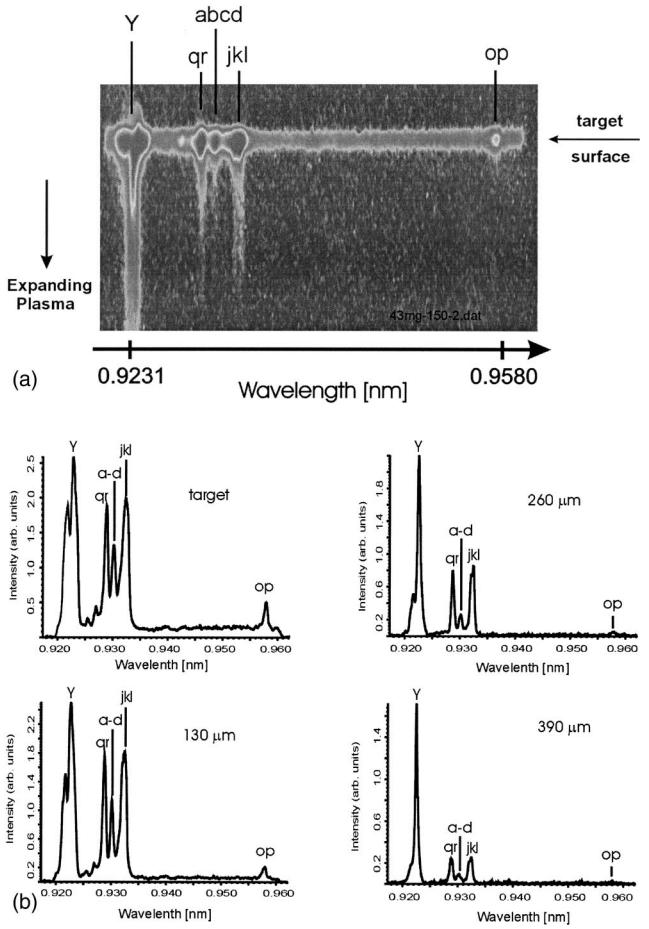

FIG. 2. (a) Spatially resolved image of the Mg-emission spectrum obtained at the nhelix laser facility. Close to the target, the Li-like *op*-satellite emissions are unusually intense. (b) Experimental Mg-emission spectra obtained from the images of (a). Close to the target, the relative emission in the *op*-satellite transitions is unusually intense, decreasing gradually with increasing target distance. Far from the target, the intensity of the *op*-satellite transitions is very small and is close to its low-density (coronal-model) value.

sponse [15], and crystal reflectivity [16]. Figure 2(a) shows the spectrally resolved plasma image. An intense emission from the Li-like *op* satellite lines can be clearly seen near the target surface, whereas far from the target this emission is essentially absent. Figure 2(b) shows some of the corresponding spectral traces for varying target distances. Close to the target, the emission from the *op* satellite lines is found to be extremely intense compared with the *jk* satellite emission. The *op*-satellite intensity decreases (relatively to that of the *jk* satellites) with increasing target distance, which was also the case in the TRIDENT experiments for silicon. The intensity of the *op* satellite transitions was found to have the expected insignificant values only far from the target, in agreement with the predictions of the theoretical models available in the literature [2,5,7]. On the basis of these new experimental observations, we suggest that a regime of cold, dense plasma near the target surface is the origin of the order-of-magnitude enhancement in the intensity of the two-electron dielectronic-satellite transitions *op* and *OP*.

III. ATOMIC DATA AND SPECTRUM SIMULATIONS

From the results obtained from experiments with completely different laser wavelengths, pulse widths, intensities, illumination geometries, and targets (massive versus foils), it has become apparent that the observed intensity enhancements of the two-electron dielectronic satellite transitions are not the result of a particular set of experimental conditions. The unexpectedly large enhancements in the relative line intensities of these transitions could lead to new opportunities for their application in plasma diagnostics. While the prominent He-like $2\ell 2\ell'$-satellite feature (J) and the Li-like $1s2\ell 2\ell'$-satellite lines (qr, $a-d$, and jkl) have been extensively employed for plasma diagnostics, the normally weak two-electron satellite transitions have not been regularly used. In order to investigate the origin of the new experimental results, we have developed a detailed, time-dependent collisional-radiative model, including radiation-transport (opacity) effects, for the relevant dielectronic satellite spectra.

Spectral simulations have been carried out using the MARIA code [17]. In this code, the atomic-level population densities are determined from a system of rate equations:

$$\frac{dn_j}{dt}=\sum_{i=l}^{N} n_i\{W_{ij}+A_{ij}+P_{ij}^{\mathrm{abs}}+P_{ij}^{\mathrm{stim}}+P_{ij}^{iz}+R_{ij}^{\mathrm{stim}}\} - n_j\sum_{k=l}^{N}\{W_{jk}+A_{jk}+P_{jk}^{\mathrm{abs}}+P_{jk}^{\mathrm{stim}}+P_{jk}^{iz}+R_{jk}^{\mathrm{stim}}\}. \tag{2}$$

The elements of the collisional-radiative transition matrix W are given by

$$W_{ij}=C_{ij}+R_{ij}+I_{ij}+T_{ij}+\Gamma_{ij}+D_{ij}, \tag{3}$$

where C denotes the collisional-excitation/deexcitation rate, I is the collisional-ionization rate, T is the three-body recombination rate, R is the (spontaneous) radiative-recombination rate, Γ is the autoionization rate, D is the radiationless electron-capture rate, A is the spontaneous radiative-emission rate, P^{iz} is the photoionization rate, P^{stim} is the stimulated radiative-emission rate, P^{abs} is the radiative-absorption rate, and R^{stim} denotes the stimulated radiative-recombination rate. The matrix elements (rate coefficients or cross sections) for the inverse processes are obtained by application of the principle of detailed balance (or microreversibility). If a particular transition cannot occur, because of energy or symmetry considerations, the corresponding rate is set equal to zero. In an alternative but equivalent collisional-radiative model including autoionizing levels [18], an explicit separation was introduced for processes occurring between adjacent stages of ionization, e.g., ionization, autoionization, electron capture, and recombination.

In order to treat the effects of radiation transport, it is convenient to combine the radiative terms A, P^{abs}, and P^{stim} according to the relationship

$$-n_jA_{ji}-n_jP_{ji}^{\mathrm{stim}}+n_iP_{ij}^{\mathrm{abs}}=-n_jA_{ji}\Lambda_{ji}. \tag{4}$$

The rate equations can then be expressed in the following alternative equivalent form:

$$\frac{dn_j}{dt}=\sum_{i=1}^{N} n_i\{W_{ij}+A_{ij}\Lambda_{ij}+P_{ij}^{iz}+R_{ij}^{\mathrm{stim}}\}-n_j \times\sum_{k=1}^{N}\{W_{jk}+A_{jk}\Lambda_{jk}+P_{jk}^{iz}+R_{jk}^{\mathrm{stim}}\}. \tag{5}$$

In our calculations, the parameter Λ_{ij} is approximated by means of an escape factor [19], including the spatial dependence $[n_j=n_j(\vec{r})]$, via the first-order approximation to the Bibermann-Holstein solution:

$$\Lambda_{ij}=\frac{1}{n_1 V}\int_0^\infty d\omega\int_\Omega\frac{d\Omega}{4\pi}\int_V dV\, n_i(\vec{r})\varphi_{ij}(\omega,\vec{r}) \times\exp[-\tau_{\omega,ij}(\vec{r},\vec{s})]. \tag{6}$$

In Eq. (6), the photon direction is specified by Ω and the optical thickness τ is defined as the integral of the absorption coefficient κ (which depends on the intensities and line shapes) from the point $\vec{r}$ inside the plasma volume to the point $\vec{s}$ on the plasma surface:

$$\tau_{\omega,ij}(\vec{r},\vec{s})=\int_{\vec{r}}^{\vec{s}}\kappa_{\omega,ij}(\vec{r}')d|\vec{r}'-\vec{r}|. \tag{7}$$

Line overlapping (also known as ''interlocking:'' see [20]) and asymmetric repumping in differentially moving plasmas (corresponding to shear flow) are incorporated by taking into account the sum of the individual line-absorption coefficients κ_{ij}:

$$\kappa(\omega)=\sum_{ij}\kappa_{ij}(\omega). \tag{8}$$

In the determination of the local (frequency-normalized) spectral-line-shape functions φ_{ij}, we have taken into account the Voigt profile, allowing for the Doppler broadening (which is specified by the ion temperature) and the Lorentz contribution. The Lorentz contribution is determined by all elementary collision and radiation processes that result in the depopulation of the upper and lower levels, e.g., radiative decay, autoionization, and electron collisional processes. Stark broadening effects, i.e., quasistatic ion-ion collisions, are included via an effective width $\Delta\omega$ (as used, e.g., in [21]):

$$\Delta\omega_1=\frac{8Ry\,\alpha Z}{1+\frac{3}{2}ZZ_R\frac{2Ry}{T_iR_Z}}\left\{\frac{\frac{n_u^2}{Q_u}-\frac{n_l^2}{Q_l}}{R_Z^2}+\frac{\frac{n_u^4}{Q_u^2}-\frac{n_l^4}{Q_l^2}}{R_Z^3}\right\}, \tag{9}$$

$$\Delta\omega_2=\frac{8Ry\,\alpha Z}{1+\frac{3}{2}ZZ_R\frac{2Ry}{T_iR_Z}}\left\{\frac{3}{2}Z\frac{\frac{n_u^7}{Q_u^3}-\frac{n_l^7}{Q_l^3}}{R_Z^4}+\frac{\frac{n_u^4}{Q_u^2}-\frac{n_l^4}{Q_l^2}}{R_Z^3}\right\}, \tag{10}$$

$$R_Z=\frac{1}{a_0}\left(\frac{3}{4\pi n_i}\right)^{1/3}. \tag{11}$$

Here $Ry=13.6$ eV, α is the fine-structure constant, $a_0=0.529\times10^{-8}$ cm, Z is the average ionic charge of the plasma, Z_R is the radiator charge, T_i is the ion temperature in eV, and n_i is the ion density in cm^{-3}. If the radiator is hydrogenic, $\Delta\omega=\Delta\omega_1$; otherwise, $\Delta\omega=\min(\Delta\omega_1,\Delta\omega_2)$. Effective charges and principal quantum numbers of the upper and lower states, Q_u, Q_l and n_u, n_l, respectively, are determined from the hydrogenic form of the ionization energies E_i:

$$E_i=\frac{Q^2Ry}{n^2}. \tag{12}$$

For autoionizing levels, E_i is taken as the energy required to remove all excited electrons. In this case, H-like transition matrix elements are found to be in good agreement with the results of Hartree-Fock calculations. We note that the effects of Stark broadening on escape factors have been considered in various limits [22].

Within the approximations of our collisional-radiative model, the influence of radiation transport is described by means of an iterative solution of the nonlinear rate equations, including the entire matrix $(W+A\Lambda+P^{iz}+R^{\mathrm{stim}})$ within the subspace of the ground states, singly excited states, and autoionizing states that have been represented. Accordingly, radiation-transport effects are simultaneously taken into account in the determination of the population densities of all included singly excited and doubly excited states as well as in the determination of the charge-state distributions, incorporating the shifts of the ionic populations due to photoabsorption processes. However, the equation of radiation transport, which describing the dynamics of the radiation-field intensity, is treated approximately by means of the escape factor method, as indicated in the above discussion. The inclusion of radiation transport is of particular importance for the autoionizing levels, because high autoionizing rates play a role similar to that of rapid collisional-depopulation rates.

The spectral distribution $I(\omega)$ of the line emission is then calculated from the full set of level-population densities, the Voigt-profile escape factors, and the normalized, optically thick line-profile functions Φ_{ij} (which are to be distinguished from the local spectral-line-profile functions that have been designated as φ_{ij}):

$$I(\omega)=\sum_{i,j}I_{ij}(\omega)=\sum_{i,j}\hbar\omega_{ij}A_{ij}\Lambda_{ij}\Phi_{ij}(\omega), \tag{13}$$

TABLE I. Atomic levels for autoionizing configurations $2\ell 2\ell'$ and $1s2l2l'$ which are included, along with other levels (ground states and excited states; see text), in a detailed collisional-radiative model. Note that the *OP*-satellite transitions originate from the $2s^2\ ^1S_0$ level, the *op*-satellite transitions originate from the $1s2s^2\ ^2S_{1/2}$ level, the *J*-satellite transition originates from the $2p^2\ ^1D_2$ level, and the *j*-satellite transition originates from the $1s2p^2[^1D]^2D_{5/2}$ level. These satellite transitions, together with other transitions, are included self-consistently in a time-dependent collisional-radiative model allowing for opacity effects.

He-like	$2s^2\ ^1S_0$, $2s2p\ ^1P_1$, $2s2p\ ^3P_0$, $2s2p\ ^3P_1$, $2s2p\ ^3P_2$, $2p^2\ ^1S_0$, $2p^2\ ^1D_2$, $2p^2\ ^3P_0$, $2p^2\ ^3P_1$, $2p^2\ ^3P_2$
Li-like	$1s2s^2\ ^2S_{1/2}$, $1s(2s2p\ ^3P)\ ^2P_{1/2}$, $1s(2s2p\ ^3P)\ ^2P_{3/2}$, $1s(2s2p\ ^3P)\ ^4P_{1/2}$, $1s(2s2p\ ^3P)\ ^4P_{3/2}$, $1s(2s2p\ ^3P)\ ^4P_{5/2}$, $1s(2s2p\ ^1P)\ ^2P_{1/2}$, $1s(2s2p\ ^1P)\ ^2P^{3/2}$, $1s(2p^2\ ^1D)\ ^2D_{3/2}$, $1s(2p^2\ ^1D)\ ^2D_{5/2}$, $1s(2p^2\ ^1S)\ ^2S_{1/2}$, $1s(2p^2\ ^3P)\ ^2P_{1/2}$, $1s(2p^2\ ^3P)\ ^2P_{3/2}$, $1s(2p^2\ ^3P)\ ^4P_{1/2}$, $1s(2p^2\ ^3P)\ ^4P_{3/2}$, $1s(2p^2\ ^3P)\ ^4P_{5/2}$

$$\Phi_{ij}(\omega)=\frac{\int_0^{L_{\rm eff}} n(x)[1-\exp(-\tau_\omega)]dx}{\int_0^\infty\int_0^{L_{\rm eff}} n(x)[1-\exp(-\tau_\omega)]dx\,d\omega}. \qquad (14)$$

The normalization procedure employed above allows for some plasma inhomogeneities.

In order to describe properly the level-population kinetics of various charge states, as well as transitions from singly excited and doubly excited states, it is necessary to adopt a rather extensive representation of the atomic-level structure in the relevant ionization stages. We have taken into account all ground states of Si *I*–Si *XV*, the H-like levels $n\ell$ with $n=1-7$ and $\ell=0-6$, the He-like levels $1sn\ell$ with $n=1-7$ and $\ell=0-6$, and the Li-like levels $1s^2n\ell$ with $n=2-7$ and $\ell=0-6$. We have employed effective dielectronic and radiative recombination rates for all charge states. For the investigation of the anomalously high relative intensities of the line emission from the He- and Li-like dielectronic-satellite transitions, it is essential to incorporate a detailed representation of the $2\ell 2\ell'$- and $1s2\ell 2\ell'$-level structures. Accordingly, we have explicitly taken into account all individual *LSJ* fine-structure levels in the atomic-kinetics model (see Table I). We note that all *LSJ*-split $2\ell 2\ell'$ and $1s2\ell 2\ell'$ levels from which, e.g., the *op, j, OP*, and *J* satellites originate, have been taken into account in the approximate treatment of the radiation-transport equation and in the detailed collisional-radiative model for atomic-level populations.

The ionization potentials of the ground states of the Si ions have been taken from Kelly [23], while the ionization energies of the excited states have been obtained from the wavelengths of particular transitions. The wavelengths, transition probabilities, and autoionizing rates have been calculated using either the relativistic Hartree-Fock-Roothaan (HFR) method, including intermediate coupling and configuration interaction [24] or the second-order multiconfiguration *Z*-expansion (MZ) procedure, including higher-order relativistic and QED effects [25–27]. All electric-dipole transitions with $\Delta S=0$, $\Delta L=\pm 1$ and $\Delta S=1$, $\Delta L=\pm 1$ have been taken into account. For a few important cases, we have also included magnetic-dipole, electric-quadrupole, and magnetic-quadrupole transitions, as well as two-photon decay processes. These higher-multipole or higher-order radiative transitions are of particular importance for the radiative emission originating from the 2ℓ and $1s2\ell$ levels of H- and He-like ions, respectively. The incorporation of these radiative transitions also permits the correct description of spectra emitted from low-density plasmas.

Since nonvanishing values of the radiative-decay rates for the *op* and *OP* satellite transitions arise only from the inclusion of configuration interaction, an accurate calculation of the configuration-mixing coefficients is essential for the correct determination of the radiative-transition amplitudes. Table II(a) shows the configuration-mixing coefficients obtained from different methods, which are found to be in very good agreement. Table II(b) shows the atomic data (wavelengths λ, radiative-transition probabilities *A*, autoionizing rates Γ, and satellite-intensity factors *Q*) for some He-like and Li-like dielectronic-satellite transitions that are of particular interest in the present investigation, i.e., the *op, jkl*, and *OP, J* transitions. The agreement among the results of these different calculations is found to be good. In particular, the satellite-intensity factors agree within 20%, even for weak transitions. Variations of the atomic data obtained from different calculations can therefore be discarded as a source of major errors in the spectral modeling.

Electron collisional-excitation cross sections have been calculated with the Coulomb-Born exchange method. The radial part has been calculated with the ATOM code [27] and the angular part has been calculated, in the intermediate-coupling scheme, with the MIXING code [28]. Electron-collisional ionization, photoionization, and dielectronic-recombination cross sections have been calculated in the Coulomb-Born exchange approximation, also using the ATOM code. Extensive comparisons with reference data available in the literature (including photoionization cross sections and dielectronic-recombination rates) show that, for highly charged ions, the results of our calculations are in good agreement. The presently calculated data are therefore believed to provide sufficient accuracy for the spectra simulations and the plasma diagnostics of highly charged ions.

IV. INTENSITIES OF THE *op* AND *OP* SATELLITE TRANSITIONS

A. Temperature and density variations in optically thin and optically thick plasmas

A change in the electron temperature can strongly influence the intensity ratios between the dielectronic satellites and resonance line, because the captured-electron energy associated with the autoionizing level is substantially different from the excitation energy of the corresponding resonance line. Under the usual plasma conditions, with electron temperatures within the range where a given ionization stage of the atomic systems has appreciable abundance in the plasma,

TABLE II. (a) Configuration mixing coefficients for the $1s2s^2\ ^2S^{1/2}$ state obtained from the present MZ and HFR calculations; see text, $Z_n=14$. (b) Atomic data for the He-like silicon satellite transitions $O=2s^2\ ^1S_0\rightarrow 1s2p\ ^1P_1+h\nu$, $P=2s^2\ ^1S_0\rightarrow 1s2p\ ^3P_1+h\nu$, and $J=2p^2\ ^1D_2\rightarrow 1s2p\ ^1P_1+h\nu$, and the Li-like satellite transitions $o=1s2s^2\ ^2S_{1/2}\rightarrow 1s^22p\ ^2P_{3/2}+h\nu$, $p=1s2s^2\ ^2S_{1/2}\rightarrow 1s^22p\ ^2P_{1/2}+h\nu$, $j=1s2p^2\ ^2D_{5/2}\rightarrow 1s^22p\ ^2P_{3/2}+h\nu$, $k=1s2p^2\ ^2D_{3/2}\rightarrow 1s^22p\ ^2P_{1/2}+h\nu$, and $l=1s2p^2\ ^2P_{3/2}+h\nu$. Very good overall agreement is obtained between different calculations. The values for the He-like ion are obtained from the MZ calculations, while the values for the Li-like ion are obtained using the HFR method.

(a)

LS state	$1s2s^2[^1S]\ ^2S_{1/2}$	$1s2p^2[^1P]\ ^2P_{1/2}$	$1s2p^2[^3P]\ ^4P_{1/2}$	$1s2p^2[^3P]\ ^2P_{1/2}$
HFR	0.94785	−0.31763	−0.01902	−0.01812
MZ	0.94882	−0.31470	−0.01903	−0.01877
Ref. [7]	0.9479	−0.3211		

(b)

Transition	λ (10^{-10} m)	A (10^{13} s^{-1})	Γ (10^{13} s^{-1})	Q (10^{13} s^{-1})
J	6.2651/6.2631	4.55/4.43	36.8/32.9	20.2/19.5
P	6.3058/6.3049	0.0233/0.0227	34.2/32.8	0.0227/0.0220
O	6.3421/6.3422	0.914/1.03	34.2/32.8	0.890/1.00
k	6.7388/6.7393	1.82/1.86	18.3/13.2	6.61/6.50
l	6.7425/6.7430	0.0576/0.0587	18.3/13.2	0.209/0.205
j	6.7432/6.7426	1.80/1.84	18.6/13.4	9.84/9.70
p	6.9027/6.9029	0.0578/0.0718	15.4/11.3	0.114/0.141
o	6.9066/6.9068	0.104/0.130	15.4/11.3	0.206/0.255

the doubly excited autoionizing states within a particular complex (e.g., the $1s2\ell2\ell'$ states) have energy differences that are much smaller than the electron temperature. Accordingly, it is expected that the relative populations of the doubly excited autoionizing levels will exhibit negligible variations with changes in T_e. The electron-temperature insensitivity of the relative populations of these autoionizing levels, which are predominantly formed by radiationless electron capture, should be contrasted with the much more pronounced electron-temperature dependence that is expected in the case of the inner-shell excited autoionizing states. We note that the inner-shell excitation and radiationless-capture processes proceed from different initial charge states. However, these temperature variations do not play a significant role in the present investigation of the He-like *OP*, *J* and Li-like *op*, *jkl* satellite transitions, because in all cases the autoionizing rates [see Table II(b)] are very large, resulting in practically constant intensity ratios as functions of the electron temperature. The rapid decrease [Fig. 3(a)] of the He_β/Ly_α intensity ratio with increasing electron temperature is caused by the larger population of higher-charge states. The He_β/He_α line-intensity ratio, however, does not vary appreciable with electron temperature, because these lines originate from the same charge state and are produced by similar excitation mechanisms. With increasing electron density [Fig. 3(b)], the He_β/Ly_α line-intensity ratio decreases because electron collisional ionization redistributes the ionic populations towards higher-charge states. It can be seen that the He_β/He_α line-intensity ratio varies only between the values of 0.1 and 0.2. This is in disagreement with the experimental spectrum (Fig. 1), which shows a much larger value for this line-intensity ratio.

The redistribution of populations among the autoionizing levels due to collisional processes is expected to be a most effective mechanism for modifying the spectral distribution of satellite transitions from upper states with significantly different autoionizing rates Γ, but with relatively high radiative-decay rates. In this collisional redistribution process, population is transferred from an autoionizing level with high Γ to levels with low Γ, from which rapid decay can occur by spontaneous radiative emission. This gives rise to a pronounced electron-density variation in the spectral distribution of the satellite transitions. Figure 3(b) shows the electron-density dependence of various line-intensity ratios. Practically no density dependence is seen for the OP/J and op/jkl satellite-intensity ratios, because in these transitions the upper states have very large autoionizing rates.

Under optically thick excitation conditions, the intensity ratios of satellites and resonance lines are not simple functions of the electron temperature alone, because the depletion of the population corresponding to the upper level of the optically thick resonance line produces a modification of the low-density line-intensity ratio. This is also the case if the effective rate for the reemission of the absorbed photon is reduced by the effects of a very high plasma density and/or a high number of photon scatterings. The influence of radiation transport, e.g., on a Doppler-broadened spectral line, can be assessed from an estimation of the line-center optical thickness τ_0 using the standard relationship

$$\tau_0 \approx 1.6\times 10^{-36}\lambda_{ji}^3\frac{g_j}{g_i}A_{ji}\sqrt{\frac{M}{kT_i}}n_iL_{\mathrm{eff}}\left(1-\frac{g_in_j}{g_jn_i}\right), \quad (15)$$

with λ in [10^{-10} m], A in [s^{-1}], n_i in [cm^{-3}], L_{eff} in [μm],

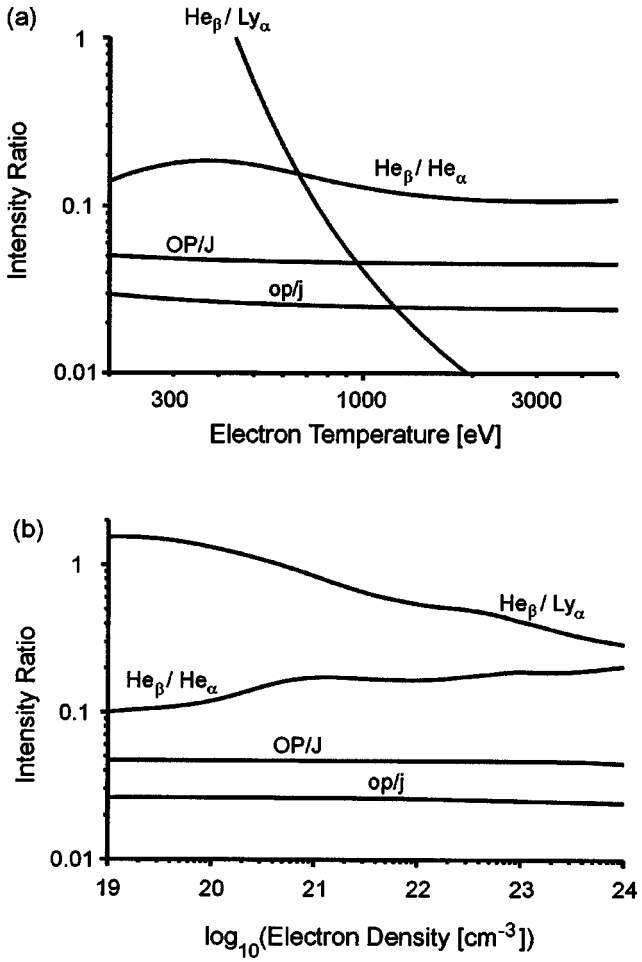

FIG. 3. Intensity ratios for silicon ($Z_n=14$) between the He_β and Ly_α lines $I(\mathrm{He}_\beta)/I(Ly_\alpha)$, the He_β and He_α lines $I(\mathrm{He}_\beta)/I(\mathrm{He}_\alpha)$, and the dielectronic-satellite lines $I(OP)/I(J)$ and $I(op)/I(jkl)$, for optically thin plasmas (a) for electron temperatures kT_e in the range 200–5000 eV and an electron density $n_e=4\times10^{21}$ cm^{-3} and (b) for an electron temperature $kT_e=500$ eV and electron densities n_e in the range 10^{19}–10^{24} cm^{-3}. The $I(OP)/I(J)$ and $I(op)/I(jkl)$ satellite-line intensity ratios are nearly independent of the temperature and density variations.

M in [amu], and kT_i in [eV]. E.g., for $kT_e=500$ eV and $n_e=4\times10^{21}$ cm^{-3} (which is the critical density in the TRIDENT experiments), and $L_{\mathrm{eff}}=500$ μm (the laser spot size), we obtain for the He-like resonance line ($\lambda=6.6485\times10^{-10}$ m, $A=3.76\times10^{13}$ s^{-1}, $g_j=3$, $g_i=1$, $n_i(1s^2)\approx1\times10^{20}$ cm^{-3}, $kT_i=kT_e$, and $M=28$): $\tau_0\approx6\times10^2$. Under such conditions, the He_β line ($\lambda=5.6808\times10^{-10}$ m and $A=1.05\times10^{13}$ s^{-1}) and even the intercombination line Y ($\lambda=6.6844\times10^{-10}$ m and $A=1.58\times10^{11}$ s^{-1}) are also optically thick. Table III shows the line-center optical-thickness values obtained including ion Doppler, electron-collisional, and Stark broadening, as well as line overlapping. The continuum optical depths in the free-free and free-bound transitions are negligible for our parameters.

The photon-absorption process plays an important role in the dielectronic-satellite transitions. Even for relatively small line-center optical-thickness values, photon absorption can have a significant influence on the line intensities of the dielectronic-satellite transitions, because the autoionizing rate plays a role similar to that of a collisional-depopulation rate [29]. E.g., for the Li-like j satellite, the probability p of reemission, following a single photon-absorption event, is given by

$$p=\frac{A}{A+C_{\mathrm{depop}}+\Gamma}. \tag{16}$$

Even for $C_{\mathrm{depop}}\ll A$, p is much less than 1 (see the atomic data in Table II). We find that $p=0.12$, whereas for a resonance line the corresponding reemission probability is close to 1. Table III shows the line-center optical depths for (a) $kT_e=300$ eV and (b) $kT_e=500$ eV. The optical depths for the Li-like satellite transitions are found to be increased [comparing cases (a) and (b)] by about a factor of 10 due to the higher populations of the Li-like levels (note that the $1s^22\ell$ levels in Li-like ions are the absorbing lower states for the Li-like $n=2$ satellites, both for dielectronic and inner-shell excited satellite transitions). It can be seen, from Table III, that the dielectronic-satellite lines *op* and *OP* have negligible opacity under almost all excitation conditions, whereas the resonance lines and even the J and j satellite lines are substantially influenced by photon-absorption processes. This in turn leads to a relative increase in the intensity of the lines with low opacity compared with the intensity of the lines with high opacity.

Figure 4 shows the electron-temperature [Fig. 4(a)] and electron-density [Fig. 4(b)] variations of selected line-intensity ratios for an optically thick plasma. For low temperatures, the op/jkl intensity ratio rises with decreasing electron temperature in optically thick plasmas. This can be understood from the increase in the population of the Li-like charge state, which results in an increase in the optical thickness of the *jkl* satellite lines, as indicated in Table III. The optical thickness of the *op* satellite lines also rises, but the absolute value of the optical thickness is still negligible. With an even further decrease in the electron temperature,

TABLE III. Calculated line-center optical-thickness values including Doppler broadening, electron collisional and Stark (static-ion) broadening, and line overlapping for a dense silicon plasma, (a) $kT_e=300$ eV, $n_e=4\times10^{21}$ cm^{-3}, $kT_e=kT_i$, $L_{\mathrm{eff}}=500$ μm (the Ly_α line contains two components, corresponding to the doublet fine-structure contributions) and (b) $kT_e=500$ eV.

		He_α	Y	He_β	Ly_α	J	O	j	q	o
(a)	τ_0	1200	6.3	120	22/44	0.2	0.020	1.6	2.8	0.049
(b)	τ_0	440	2.3	45	110/220	0.49	0.035	0.31	0.54	0.0032

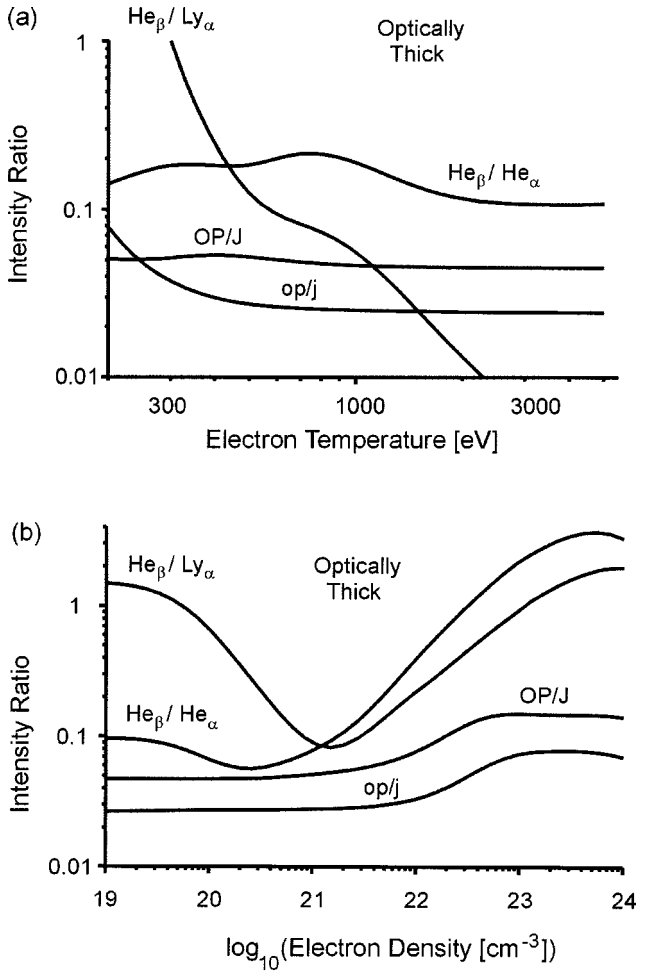

FIG. 4. Intensity ratios for silicon ($Z_n=14$) between the He_β and Ly_α lines $I(He_\beta)/I(Ly_\alpha)$, the He_β and He_α lines $I(He_\beta)/I(He_\alpha)$, and the dielectronic-satellite lines $I(OP)/I(J)$ and $I(op)/I(jkl)$, for optically thick plasmas (a) for electron temperatures kT_e in the range 200–5000 eV, an electron density $n_e=4\times10^{21}$ cm^{-3}, and $L_{\rm eff}=500$ μm and (b) for an electron temperature $kT_e=500$ eV, electron densities n_e in the range 10^{19}–10^{24} cm^{-3}, and $L_{\rm eff}=500$ μm.

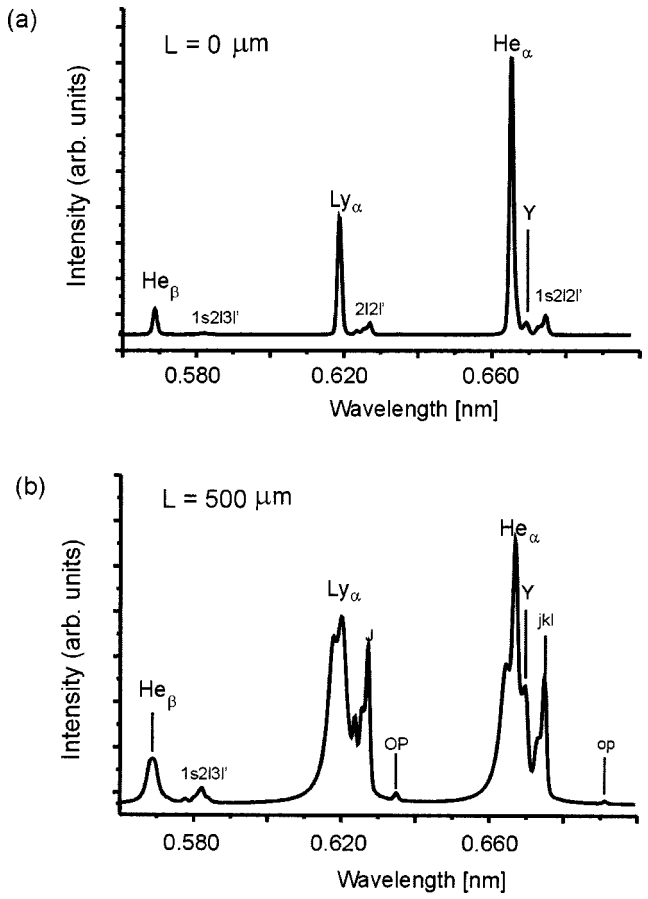

FIG. 5. Simulated TRIDENT silicon line-emission spectra, including Stark broadening and line overlapping, from 0.56 to 0.70 nm, $kT_e=600$ eV, $n_e=6\times10^{21}$ cm^{-3}, for an optically thin plasma (a) and an optically thick plasma ($L_{\rm eff}=500$ μm) (b). The photon absorption of lines with large oscillator strengths results in a relative increase in the intensity of the *OP* and *op* dielectronic satellites in the line-emission spectrum.

the abundance of the Li-like ions again decreases. However, this parameter regime is not of interest for the present investigation.

In Figs. 3(b) and 4(b), the electron-density variations of the selected line-intensity ratios are shown for optically thin and optically thick plasmas, respectively. In optically thick plasmas, the decrease of the He_β/Ly_α intensity ratio is even more pronounced due to the collisional ionization from the photopumped $1s2\ell$ levels [see the density region $n_e=10^{19}$–10^{21} cm^{-3} of Fig. 4(b)]. For even higher densities, the increasing opacity of the Ly_α line produces a corresponding increase in the intensity ratio. A high opacity in the *J* and *j* satellite lines is the cause (see Table III) for the rise of both the OP/J and op/jkl intensity ratios [see Fig. 4(b), $n_e\approx3\times10^{22}$ cm^{-3}]. A higher opacity in the He_α line, relative to He_β, can lead to intensity ratios much larger than about 0.1–0.2 [see Fig. 4(b)] at about $n_e=10^{20}$ cm^{-3} and $n_e=3\times10^{22}$ cm^{-3}. Note that for He_β the radiative-recombination-induced intensity is small [30].

Figure 5 shows the spectral simulations obtained for silicon in the spectral range from 0.56 to 0.70 nm for an optically thin [Fig. 5(a)] and optically thick [Fig. 5(b)] plasma. For optically thick plasmas, extended wings develop for the Ly_α and He_α lines. This is a result of a large opacity (see Table III) and the effects of Stark broadening (see also the extended wings in the observed spectrum in Fig. 1). In the optically thick case, an increase can be seen in the relative importance of the *OP* and *op* satellite transitions: with increasing density, the satellite-intensity ratios rise from the coronal-model values of 0.047 and 0.026 (Fig. 3) to about 0.15 and 0.068 [Fig. 4(b)], respectively. However, these increased values are much too small to account for the new experimental results (Figs. 1 and 2), which show order-of-magnitude higher intensity ratios than predicted by the results in Fig. 3.

B. Transient-line formation

We have carried out time-dependent spectral simulations for the radiative emissions in the *op* and *OP* dielectronic-

satellite transitions, assuming various values for the basic plasma parameters. The results of these simulations show that transient effects alone cannot account for the unexpectedly high satellite-line intensities, neither in any of the time intervals nor in the time-integrated spectra obtained by superimposing all transient snap shots. This conclusion can be understood from the observation that the inner-shell excitation mechanism, which is expected to provide a more substantial contribution in an ionizing plasma, plays a negligible role under the conditions of our experiments.

C. Influence of hot electrons

The effects of hot electrons on the line-formation process are investigated by taking into account the additional (nonthermal) electron-ion collisional processes in the kinetics description (i.e., in the collisional-radiative transition matrix W). For a demonstration of the principal effects of hot electrons on the line-emission spectra, we find it convenient to define a hot-electron fraction according to

$$f_{\mathrm{hot}}=\frac{n_{\mathrm{hot}}}{n_{\mathrm{cold}}+n_{\mathrm{hot}}}. \tag{17}$$

The collision rate coefficients are modeled by

$$\langle V\sigma\rangle=(1-f_{\mathrm{hot}})\langle V\sigma,T_{\mathrm{cold}}\rangle+f_{\mathrm{hot}}\langle V\sigma,T_{\mathrm{hot}}\rangle, \tag{18}$$

where the notation $\langle V\sigma,T\rangle$ indicates the average (integration) of the collision rate $V\sigma$ over the electron-energy distribution function (which at present is assumed to be a Maxwellian corresponding to the temperature parameter T):

$$\langle V\sigma,T\rangle=\int_{E_0}^{\infty}\sigma(E)V(E)F(E)dE, \tag{19}$$

where

$$F(E)=\frac{2}{\sqrt{\pi}}\sqrt{E}\frac{\exp(-E/kT)}{(kT)^{3/2}}. \tag{20}$$

This model has been referred to as a two-temperature approach. For the three-body recombination process, the corresponding expression for the collision rate coefficients is much more complicated due to the occurrence of two electron-energy distribution functions in the expression for the double collisional-ionization rate coefficient:

$$\langle V\sigma^{\mathrm{tr}}\rangle=(1-f_{\mathrm{hot}})^2\langle V_1V_1\sigma^{\mathrm{tr}}\rangle+f_{\mathrm{hot}}^2\langle V_2V_2\sigma^{\mathrm{tr}}\rangle+2\,f_{\mathrm{hot}}(1-f_{\mathrm{hot}})\langle V_1V_2\sigma^{\mathrm{tr}}\rangle, \tag{21}$$

where

$$\langle V_kV_l\sigma_{ji}^{\mathrm{tr}}\rangle=\frac{\pi^2\hbar^3}{m_e^2}\frac{g_i}{g_j}\int_0^{\infty}dE_k\int_0^{\infty}dE_l\times\frac{E}{\sqrt{E_kE_l}}\sigma_{ij}^{l}(E,E_k)F(E_k)F(E_l). \tag{22}$$

If $k=l$, the integral in Eq. (22) can be reduced to an integration over the usual (ground-state) ionization cross section $\sigma^I(E)$ (physically, this is equivalent to the application of the principle of detailed balance). For $k\neq l$, the integrals must be performed numerically over the double-differential ionization cross section $\sigma_{ij}^{I}(E,E_k)$. This involves a substantial computational effort.

Since the presence of hot electrons preferentially results in enhanced inner-shell excitation and inner-shell ionization rates, we have augmented our collisional-radiative model to include additional inner-shell collision processes. Specifically, we have taken into account the inner-shell ionization processes

$$\text{(i)}\quad 1s^22\ell+e^-\rightarrow 1s2\ell+2e^-,$$

$$\text{(ii)}\quad 1s^22s2p+e^-\rightarrow 1s^22p+2e^-,$$

$$\text{(iii)}\quad 1s^22\ell2\ell'+e^-\rightarrow 1s2\ell2\ell'+2e^-.$$

The first inner-shell ionization process gives rise to increased spectral intensities for the W ($1s2p\ ^1P_1-1s^2\ ^1S_0$) and Y ($1s2p\ ^3P_1-1s^2\ ^1S_0$) emission lines, while the third process directly populates the upper states of the Li-like dielectronic-satellite transitions from the configurations $1s2\ell2\ell'$. The inner-shell excitation process is often an important mechanism for the collisional excitation of the autoionizing levels: Accordingly, we have taken into account the additional inner-shell excitation processes

$$\text{(i)}\quad 1s^22\ell+e^-\rightarrow 1s2\ell2\ell'+e^-,$$

$$\text{(ii)}\quad 1s2\ell+e^-\rightarrow 2\ell2\ell'+e^-.$$

Figure 6 shows the intensity ratios as functions of the hot-electron fraction for $n_e=10^{22}$ cm^{-3}, $kT_{\mathrm{bulk}}=300$ eV, and $kT_{\mathrm{hot}}=10$ keV. With increasing hot-electron fraction, the $\mathrm{He}_\beta/Ly_\alpha$ intensity ratio decreases (as indicated by a comparison of Figs. 3 and 4) because an increase in the hot-electron fraction redistributes the population densities toward higher charge states. The op/j and OP/J intensity ratios are not significantly affected by hot electrons, as indicated in Fig. 6(a). This observation demonstrates that, in the range of plasma parameters of interest, the inner-shell collisional processes do not significantly enhance the population densities of the upper doubly excited states $1s2s^2\ ^2S_{1/2}$ and $2s^2\ ^1S_0$ in comparison with those of the other autoionizing doubly excited states $1s2\ell2\ell'$ and $2\ell2\ell'$. In optically thick plasmas [Fig. 6(b)], the op/j satellite-intensity ratio decreases with increasing hot-electron fraction, because higher hot-electron fractions reduce the lower-state population densities in the j-satellite transition. Under these conditions, no significant increases in the op/j and OP/J intensity ratios are observed.

V. CHARGE TRANSFER

A. Charge transfer as a population mechanism for the autoionizing states

Experiments were performed using thin foils and massive targets at the GSI nhelix-laser facility. These experiments

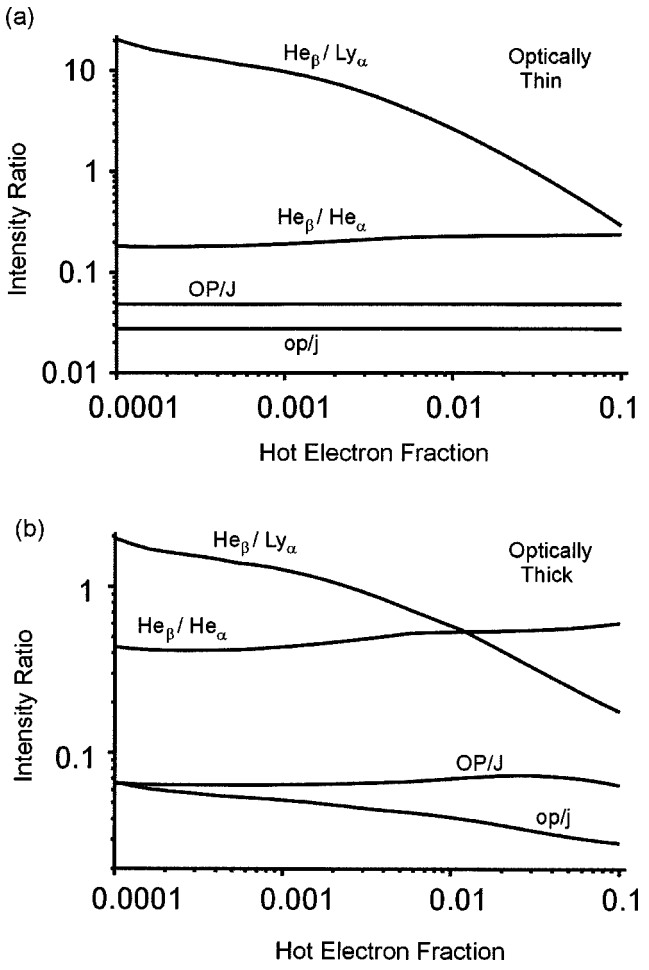

FIG. 6. Line intensity ratios for non-Maxwellian plasmas, indicating the dependence on the hot-electron fraction f_{hot}, for an optically thin plasma (a) and an optically thick plasma (b), with $n_e = 10^{22}$ cm^{-3}, $kT_{\mathrm{bulk}} = 300$ eV, $kT_{\mathrm{hot}} = 10$ keV, and $Z_n = 14$.

featured the simultaneous observation of emission spectra and pinhole images from the front and back sides of the target. The results of this simultaneous observation indicate that plasma jets are ejected not only in the backward direction but also in the forward direction. Since this phenomenon was also observed in the TRIDENT experiments with single-sided illumination of 20-μm thin foils, we are lead to an interpretation involving the mixing of different types of plasmas. Specifically, we suggest that plasma jets containing highly charged ions are mixing with plasmas containing weakly ionized ions. Plasma jets are usually associated with the existence of hot electrons. Evidence for hot electrons can be seen in the K_α emission spectra obtained from the TRIDENT experiment, which is shown in Fig. 1, and also in the spectra from the nhelix experiments with massive Al targets. The self-generated magnetic fields are most probably responsible for the production of an electron return current that impinges upon the target, as in an x-ray tube.

During this interpenetration of the two different types of plasmas discussed above, electron charge-transfer processes can take place from relatively low-charged ions to highly charged ions in the plasma jet. The geometry for these

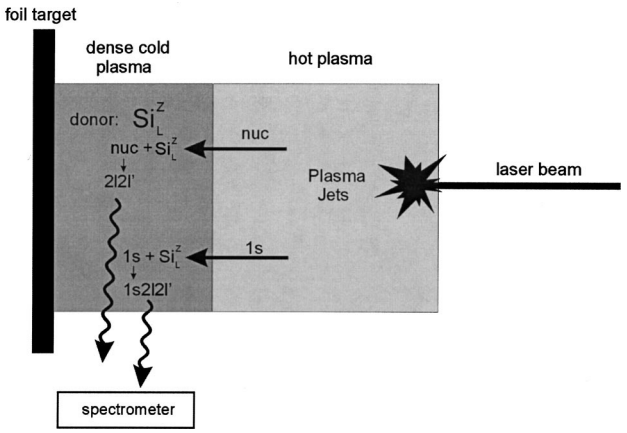

FIG. 7. Schematic illustration of the model adopted for electron charge transfer initiated by the interpenetration of the hot and cold plasma volumes (driven by jets). Double-electron charge-transfer processes (nuc, 1*s* indicate the acceptor ions, Si_L^Z the donor ion) may lead to a direct population of the autoionizing states $2\ell 2\ell'$ and $1s2\ell 2\ell'$, from which, e.g., the dielectronic-satellite transitions *OP*, *op*, *J*, and *j* originate.

charge-transfer processes is illustrated in Fig. 7 for one side of the target in the TRIDENT experiments. In this nonequilibrium environment, highly ionized silicon plasma jets (consisting of *K*-shell ions: nuclei, H-like, and He-like; which will be designated as Si_K^Z in the following discussion) undergo charge-transfer processes with *L*-shell silicon ions (e.g., B-, C-, and N-like ions, which will be designated as Si_L^Z) near the target surface.

It is informative to consider the states that are preferentially populated as a result of collisions between highly charged ions (e.g., fully stripped silicon colliding with Li-like silicon, $Z = 14$, $I = 0.5$ keV). These states can be characterized by an effective principal quantum number n_f [31], which is defined as follows:

$$n_f \approx \sqrt{\frac{Ry}{I}}\, Z \sqrt{\frac{2\sqrt{Z}+1}{Z+2\sqrt{Z}}} \approx 2.5, \tag{23}$$

where Z is the charge of the ions Si_K^Z and I is the ionization potential (in eV) of the ions, Si_L^Z. This estimate for the effective principal quantum number is found to be in good agreement with the results of calculations using the code described by Tolstikhina and Shevelko [32]. Figure 8 shows the energy-dependent charge-transfer cross sections for the most important quantum numbers $n = 1-8$. This figure shows the dominance of the charge-transfer processes involving transitions into the $n = 2$ and 3 quantum states over the entire energy range. This result implies that excited states with relatively low quantum numbers are populated preferentially by this charge-transfer process.

We note that the ionization potentials of the $1s^2 2s^2 2p^n$ states are rather similar [e.g., E_i(B-like) = 0.4 keV, E_i(C-like) = 0.35 keV, and E_i(N-like) = 0.3 keV]. Consequently, it is necessary to consider not only the single-electron charge-transfer process, but also the double-electron charge-transfer process. It can be anticipated that double-

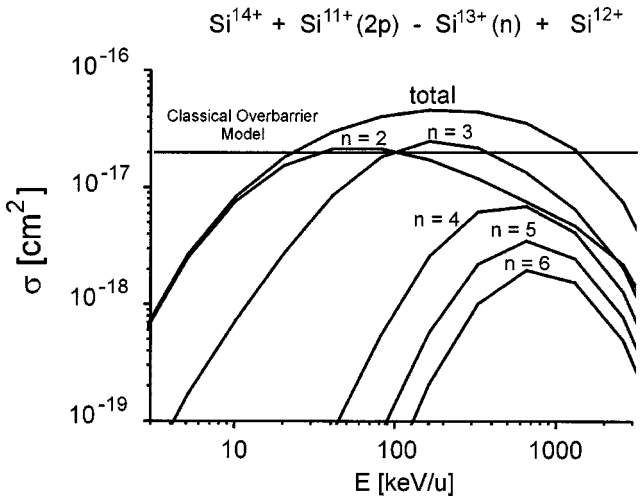

FIG. 8. Single-electron charge-transfer cross sections for ion-ion collisions from Li-like silicon to fully stripped silicon for different energies (keV per nucleon) and principal quantum numbers n. Charge transfer occurs preferentially into the $n=2$ and $n=3$ states. Also indicated is the cross-section value predicted using the classical over-barrier model (see text).

electron charge exchange could play an important role, because this process directly populates the autoionizing levels $2\ell 2\ell'$ and $1s2\ell 2\ell'$ through capture from ground ions:

$$\mathrm{nuc}+\mathrm{Si}_L^Z \rightarrow 2\ell 2\ell' + \mathrm{Si}_L^{Z-2},$$

$$1s+\mathrm{Si}_L^Z \rightarrow 1s2\ell 2\ell' + \mathrm{Si}_L^{Z-2}.$$

These charge-transfer processes therefore represent an additional population mechanism for the upper autoionizing states in the He- and Li-like dielectronic-satellite transitions. To the best of our knowledge, these processes have not been previously considered as a population mechanism for autoionizing states in dense plasmas.

Unfortunately, the required double-electron charge-exchange cross sections are not available in the literature. Accordingly, we have estimated the single-electron and double-electron cross sections using the classical over-barrier model [33]:

$$\sigma_1 \approx \pi a_0^2 (R_1^2 - R_2^2), \quad \sigma_2 \approx \pi a_0^2 (R_2^2 - R_3^2), \tag{24}$$

with

$$R_1 \approx 2Ry\,\frac{2\sqrt{Z}+1}{I_1}, \quad R_2 \approx 2Ry\,\frac{2\sqrt{Z-1}+1}{I_2},$$

$$R_3 \approx 2Ry\,\frac{2\sqrt{Z-2}+1}{I_2}, \tag{25}$$

where I_1 and I_2 are the ionization potentials in [eV] of the donor atomic systems. It is desirable to obtain an indication of the expected accuracy of the cross sections obtained from this classical model. Figure 8 includes a comparison of the results obtained using this model, with the results of detailed numerical calculations. At the cross-section maximum, the results differ at most by a factor of about 2. At its peak, the energy-dependent cross section is seen to be very large, $\sigma = 4\times 10^{-17}$ cm^2. In addition, very large cross sections ($\sigma \geqslant 10^{-18}$ cm^2) are encountered over a broad energy interval 90 keV$<E<$1.4 MeV. (Note that the energy scale in Fig. 8 is given in keV per nucleon.) Such energies are usually encountered in plasma jets produced by high-intensity lasers. We have also estimated the double-electron charge-transfer cross sections. For relatively low-charged silicon donor ions with ground-state ionization potentials of I_1(C-like) $=351$ eV, I_2(B-like)$=401$ eV, and I_3(Be-like)$=476$ eV colliding with completely ionized silicon acceptor ions, $Z=14$, we obtain for the total cross sections $\sigma_1 = 1.1\times 10^{-17}$ cm^2 and $\sigma_2 = 9.2\times 10^{-18}$ cm^2. An estimate of the accuracy of the above cross-section values can be made, evaluating σ_1 and σ_2 by means of the scaling relations deduced from the numerous experimental data that have been obtained from positive rare-gas ions penetrating into neutral rare and molecular gases [34]: $\sigma_1 = 2.7\times 10^{-18}$ cm^2 and $\sigma_2 = 5.3\times 10^{-19}$ cm^2. The cross sections obtained by means of these two different approximations are found to differ by about a factor of 4/20; deviations of this order are not expected to be significant for the present investigation. The charge-transfer cross sections in ion-ion collisions are very large above threshold, because we have considered reaction partners for which the ionization energy of the acceptor-ion partner is much larger than that of the donor ion. In this case, classically allowed over-barrier transitions can occur. These transitions are distinctly different from reactions, such as $\mathrm{He}^{2+}+\mathrm{C}^{5+}\rightarrow \mathrm{He}+\mathrm{C}^{6+}$, where transitions can take place under the barrier with correspondingly small cross sections [35]. Finally, calculations [36] show that, for energies above a few times the cross-section maximum, the ion-ion cross sections essentially coincide with those for the corresponding ion-atom collision.

We therefore suggest that the cross sections for single-electron and double-electron charge-exchange encounters between ions may be quite large and close to the corresponding ion-atom cross sections. Due to the unavailability of numerical results for the specific required ion-ion cross sections, it seems reasonable to express the desired ion-ion cross sections in the form of the following product:

$$\sigma_{ij}^{Cx}(\text{ion-ion}) = \sigma_{ij}^{Cx}(\text{atom-ion})\,k_\sigma\,. \tag{26}$$

Here σ(ion-ion) is the required, but not available, ion-ion charge-transfer cross section, σ(atom-ion) is the cross section for the corresponding atom-ion collision calculated with the over-barrier model [Eqs. (24) and (25)], and k_σ is a correction factor. Due to the Coulomb repulsion, k_σ can be much less than unity for small relative velocities (see above). For large relative velocities, the ion-ion charge-exchange cross section is found to exhibit the same behavior as the corresponding ion-atom cross-section and k_σ is then of the order of unity. For very high energies, the ion-ion charge-exchange cross section is found to decrease. We therefore treat k_σ as an adjustable parameter.

B. ℓ distribution of autoionizing-level population produced by charge transfer

Unfortunately, no calculations or experiments have been carried out for the required charge-exchange cross sections associated with the specific L, S, and J quantum numbers specifying the individual autoionizing states. In order to investigate the sensitivity of the OP/J and op/jkl satellite-line intensity ratios to the distribution of autoionizing-level populations over the angular momentum quantum number ℓ, we have selected three different models: the projection of the parabolic quantum number (model 1), the successive weak-field limit (model 2), and the statistical distribution (model 3).

1. Model 1

In order to investigate the mechanisms responsible for the establishment of the autoionizing-level LS distributions, we consider first the single-electron capture process. In the low-energy range, the collision velocity is assumed to be small compared with the orbital-electron velocity. The dynamics of the electron-capture process can then be described by adopting a quasistatic picture of the electron dynamics under the influence of the fields created by two Coulomb centers, due to the ion-core potentials. Electron transfer is usually associated with adiabatic tunneling of the electron from the target ion to the projectile ion. Due to the strong Coulomb interaction of the electron with both ion-core centers, the initially populated ℓ states undergo appreciable Stark mixing. Consequently, the single-electron states can be adequately represented by parabolic wave functions. These parabolic (Stark) states are strongly asymmetric, in contrast with the initial, spherical (unperturbed) ℓ states. The electron wave functions are elongated towards the neighbor center. This behavior is manifest by the nonzero electric-dipole matrix elements characteristic of the parabolic single-electron states. The electron undergoing the tunneling transition is most likely to occupy a similarly elongated state on the projectile ion. Mathematically, this property can be described in terms of conservation of the nodes of the quasiradial wave function and also in terms of the well-known von Neumann–Wigner theorem restricting the occurrence of quasimolecular crossings (and pseudocrossings). In our description, we assume that the electron-capture process leads to the preferential population of the final single-electron states with parabolic numbers $n_1=0$, $n_2=n-1$ [33]. Then, for single-electron capture processes, the ℓ distribution is given by the Clebsch-Gordan coefficients of the transformation from parabolic to spherical single-electron states. Returning to two-electron exchange, we assume that the two-electron state for the captured electrons can be represented as the product of two parabolic single-electron states $|n_1,n_1-1,0\rangle$ and $|n_2,n_2-1,0\rangle$. The final result is obtained by the direct evaluation of the projection $\langle \ell_1,\ell_2,LS|n_1,n_1-1,0;n_2,n_2-1,0\rangle$. These matrix elements are easily expressed in the form of the sum of the relevant Clebsch-Gordan coefficients or $3j$ symbols. It should be noted that, independent of the applicability of this picture, there will be some restrictions on the LS level-population distribution, because the resulting magnetic quantum numbers are likely to be zero. This inhibits the domination by high-L states, which have the largest statistical weights. The probability distribution W (which should not be confused with the transition matrix introduced earlier) is then given by

$$W(n_1l_1,n_2l_2)=g(S)[\xi(n_1l_1)\xi(n_1l_1)\mu(l_1,l_2,L)]^2, \tag{27}$$

$$\xi(nl)=C^{[(n-1)/2][(n-1)/2]l}_{[(n-1)/2][(n-1)/2]0}, \tag{28}$$

$$\mu(l_1,l_2,L)=C^{l_1\,l_2\,L}_{0\,0\,0}, \tag{29}$$

$$C^{j_1\,j_2\,j_3}_{m_1\,m_2\,m_3}=(-1)^{m_3+j_1-j_2}\sqrt{2j_3+1}\begin{pmatrix} j_1 & j_2 & j_3 \\ m_1 & m_2 & m_3 \end{pmatrix}. \tag{30}$$

For $n_1\neq n_2$,

$$g(S)=\frac{2S+1}{4}. \tag{31}$$

However, for $n_1=n_2$, only $S=0$ is permitted and we have

$$g(l_1,l_2)=\begin{pmatrix} 2 & \text{if } l_1\neq l_2, \\ 1 & \text{if } l_1=l_2 \end{pmatrix}. \tag{32}$$

We obtain $W(2p^2\ ^1D_2)=\frac{1}{6}=0.167$. This value should be compared with $W(2s^2\ ^1S_0)=\frac{1}{4}=0.25$. Similar relations pertain for the Li-like autoionizing configurations $W(1s2p^2\ ^2D_{5/2})=\frac{1}{6}\times\frac{1}{2}=0.0833$, which should be compared with $W(1s2s^2\ ^2S_{1/2})=\frac{1}{4}=0.25$.

2. Model 2

Characteristic interpenetration velocities that are due to conventional hydrodynamic expansion are expected to be of the of the order of 10^6–10^7 cm/s (in the case of plasma jets, these velocities may be one to two orders of magnitude higher). These interpenetration velocities are below one atomic-velocity unit. In the single-electron charge-exchange process, the distribution $W_{n\ell}$ over ℓ is given in the weak-field limit by [37–39]

$$W_{nl}=\frac{2l+1}{(n+l+1)!}\frac{\{(n-1)!\}^2}{(n-l-1)!}. \tag{33}$$

For the respective states of interest, we thereby obtain $W_{2s}=1/2$ and $W_{2p}=1/2$. Assuming that the two-electron transfer process can be described as a succession of two independent single-electron transfers occurring to the states described by spherical quantum numbers [Eq. (33)], the corresponding two-electron distribution can be represented as a product of the two individual single-electron distribution $W_{n\ell}$. We then obtain the following results: the $2s^2$ and $1s2s^2$ states are populated with a probability of 0.25, the $2s2p$ and $1s2s2p$ states are populated with a probability of 0.5, and the $2p^2$ and $1s2p^2$ states are populated with a probability 0.25. This leads to a preferential population of the $2s^2$ and $1s2s^2$ states, because only one fine-structure state can be formed from

each of these electronic configurations: namely, the $2s^2\ ^1S_0$ and $1s2s^2\ ^2S_{1/2}$ states, respectively. For processes leading to population of the other electronic configurations $2\ell 2\ell'$ and $1s2\ell 2\ell'$, this population is distributed among several final *LSJ* levels. In particular, the probability factor for the $2p^2\ ^1D_2$ autoionizing level (which is the upper level in the *J* satellite transition) is $W(2p^2\ ^1D_2)=\frac{1}{4}\times\frac{5}{15}=0.0833$. This value should be compared with $W(2s^2\ ^1S_0)=\frac{1}{4}\times\frac{1}{1}=0.25$. Similar relations are obtained for the Li-like autoionizing levels: $W(1s2p^2\ ^2D_{5/2})=\frac{1}{4}\times\frac{6}{30}=0.05$. This relation should be compared with $W(1s2s^2\ ^2S_{1/2})=\frac{1}{4}\times\frac{1}{1}=0.25$. Double-electron charge transfer can therefore lead to a preferential population of the $2s^2\ ^1S_0$ and $1s2s^2\ ^2S_{1/2}$ states in dense plasmas. This result is based on the assumption that the double-electron charge-transfer process can be adequately described by the above approximation for $W_{n\ell}$.

3. Model 3

In view of these uncertainties in the theoretical models, we are lead to consider the limiting case of statistical level populations: $W(2p^2\ ^1D_2)=\frac{5}{28}=0.179$. This value should be compared with $W(2s^2\ ^1S_0)=\frac{1}{28}=0.0357$. Similar relations are obtained for the Li-like autoionizing levels: $W(1s2p^2\ ^2D_{5/2})=\frac{6}{56}=0.107$, which should be compared with $W(1s2s^2\ ^2S_{1/2})=\frac{2}{56}=0.0357$.

C. Incorporation of charge-transfer processes in a detailed collisional-radiative model

Charge-transfer processes can be self-consistently taken into account in the description of the atomic-level population kinetics. Specifically, the shift of the ionic-level populations can be determined self-consistently with the increase in the upper-level populations due to selected charge-exchange processes. The following processes have been included self-consistently in a detailed collisional-radiative model:
Single-electron capture:

$$\mathrm{nuc}+\mathrm{Si}_L^Z\rightarrow nl+\mathrm{Si}_L^{Z-1},$$

$$1s+\mathrm{Si}_L^Z\rightarrow 1snl+\mathrm{Si}_L^{Z-1},$$

$$1s^2+\mathrm{Si}_L^Z\rightarrow 1s^2nl+\mathrm{Si}_L^{Z-1}.$$

Double-electron capture:

$$\mathrm{nuc}+\mathrm{Si}_L^Z\rightarrow nln'l'+\mathrm{Si}_L^{Z-2},$$

$$1s+\mathrm{Si}_L^Z\rightarrow 1snln'l'+\mathrm{Si}_L^{Z-2},$$

$$1s^2+\mathrm{Si}_L^Z\rightarrow 1s^2nln'l'+\mathrm{Si}_L^{Z-2}.$$

The rate coefficient *x* can be evaluated using the relationship

$$x_{ij}=f_{cx}n_eV\sigma_{ij}^x k_\sigma, \tag{34}$$

where n_e is the electron density, *V* the relative velocity of the ions undergoing charge exchange, σ^x is the corresponding charge-exchange cross section multiplied by the ℓ-distribution probability factor *W* discussed above, *i* and *j* specify the quantum states in the acceptor ion Si_K^Z, and f_x is the effective donor-ion fraction given by

$$f_x=\frac{n_i^{\mathrm{donor}}}{n_e}. \tag{35}$$

Here n_i is the density of the donor ions Si_L^Z. The transition matrix *W* may now be expressed in the form

$$W_{ij}=C_{ij}+R_{ij}+I_{ij}+T_{ij}+\Gamma_{ij}+D_{ij}+x_{ij}. \tag{36}$$

Charge-transfer processes are thereby included in the detailed collisional-radiative model, together with all other collisional and radiative processes described above. We note that the incorporation of the double-electron charge-transfer cross section requires special attention. The usual kinetic processes, e.g., ionization, three-body recombination, radiative recombination, photo-ionization, dielectronic capture, and autoionization, connect neighboring charge states. However, the double-electron charge-transfer process connects ions with charges *Z* and $(Z-2)$. Consequently, simple block-diagonal methods for the matrix inversion can be expected to be inadequate. Accordingly, we have employed a full matrix-inversion scheme with iteration, without any block-diagonal approximations.

Figure 9 shows the numerical results of our calculations, using the ℓ-distribution model 2 for optically thin [Fig. 9(a)] and optically thick [Fig. 9(b)] plasma conditions corresponding to $kT_e=700$ eV and $n_e=10^{22}$ cm^{-3}. Due to the unavailability of theoretical and experimental results for the required charge-transfer cross sections, we have tentatively assumed that $k_\sigma=1$ in Eq. (26). With increasing charge-exchange fractions, the $\mathrm{He}_\beta/Ly_\alpha$ intensity ratio rises. This can be attributed to the shift of the ionic-level populations toward lower charge states, whose populations are determined self-consistently with the excited-state populations. As an illustration, for $f_x=10^{-9}$ and $n_e=10^{22}$ cm^{-3} (i.e., $n_i^{\mathrm{donor}}=10^{13}$ cm^{-3}), the number of donor ions in a sphere with a diameter of 500 μm (corresponding to the focal spot size) is 10^9. This number of donor ions can be easily realized in plasma jets. In optically thin plasmas, the OP/J and op/j intensity ratios rise by a factor of about 2 [this should be compared with, e.g., the intensity ratios shown in Fig. 9(a) for $f_x=10^{-11}$ and $f_x=10^{-9}$]. A very interesting behavior can be seen in the results obtained for optically thick plasmas [Figs. 9(b) and 4(b)]: for $f_x=10^{-9}$ the intensity ratios show a rise by an amount up to about 0.2–0.3, which is about 10 times that obtained without the inclusion of charge-transfer processes [as indicated by the arrow in Fig. 9(b)]. This distinct difference between the results obtained for optically thin and optically thick plasmas can be understood from the fact that the intensities of the *J*- and *jk*-satellite lines are significantly influenced by photon-absorption processes. Due to the high autoionizing rates of the upper levels in these satellite transitions, any additional population of these states is therefore not directly reflected in the emission spectrum. A contrasting behavior can be seen for the *OP*-and *op*-satellite lines. In almost all parameter regimes, these satellite lines are

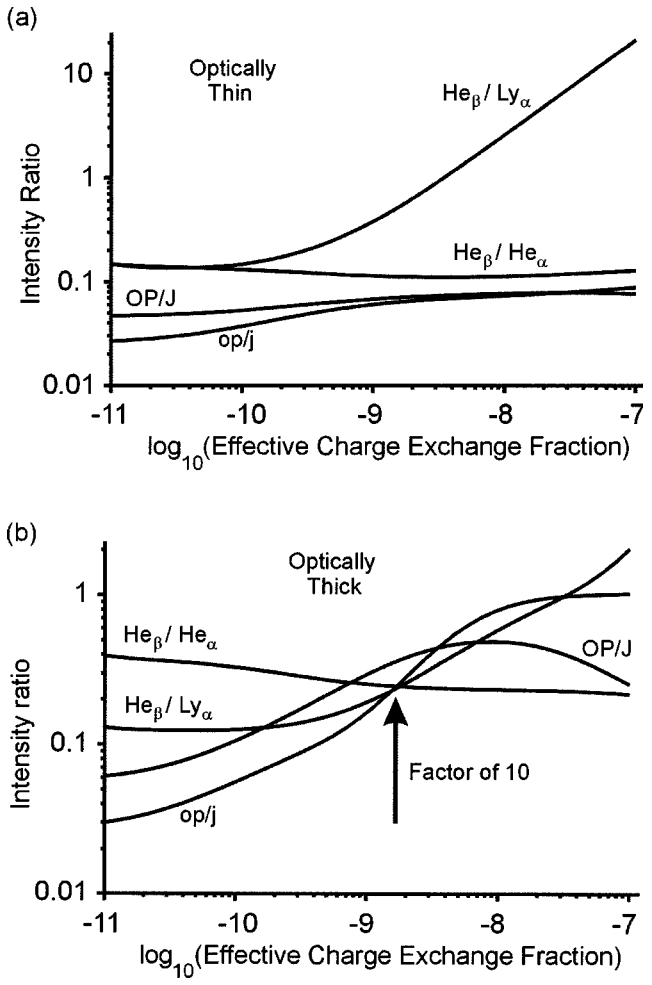

FIG. 9. Line-intensity ratios in charge-transfer-coupled plasmas, as functions of the cold donor-ion fraction (relative to the electron density). The interpenetration velocity $V=10^8$ cm/s, the electron density $n_e=10^{22}$ cm^{-3}, and the electron temperature $kT_e=700$ eV. Single-electron and double-electron charge-transfer processes proceed from cold silicon plasmas containing ions in the electronic configurations $1s^2 2s^2 2p^3$, $1s^2 2s^2 2p^2$, and $1s^2 2s^2 2p^1$ (a) for an optically thin plasma and (b) for an optically thick plasma, $L_{\text{eff}}=500$ μm.

optically thin, and any additional population mechanism will result directly in increased line intensities in the emission spectrum.

We note that the behavior described above is fully consistent with the TRIDENT observations, for which the anomalous intensities of the *OP* and *op* satellite transitions occur only near the target surface. For specific physical conditions, we encounter a high optical thickness and a sufficient amount of Si_L^Z ions from the cold plasma near the target. Our numerical results show that, e.g., for temperatures of $kT_e=100$ eV, $n_e=10^{22}$ cm^{-3}, and $L_{\text{eff}}=500$ μm, the relative fraction of the Be-, B-, C-, and N-like ions is about $10^{-2}-10^{-3}$. The absolute values of the fraction f_x in Fig. 9 have no direct meaning, because we have set k_σ equal to unity (due to the unavailability of more accurate estimates for the cross sections), as discussed above. The rise of the op/j and OP/J intensity ratios, however, occurs for donor-ion fractions of the order of 10^{-9}. These low fractions enable the reduction factor k_σ to account for the influence of Coulomb repulsion at lower energies, as well as for only fractional contributions from some ions to the recorded spectra. This allows the additional level-population mechanism to become effective.

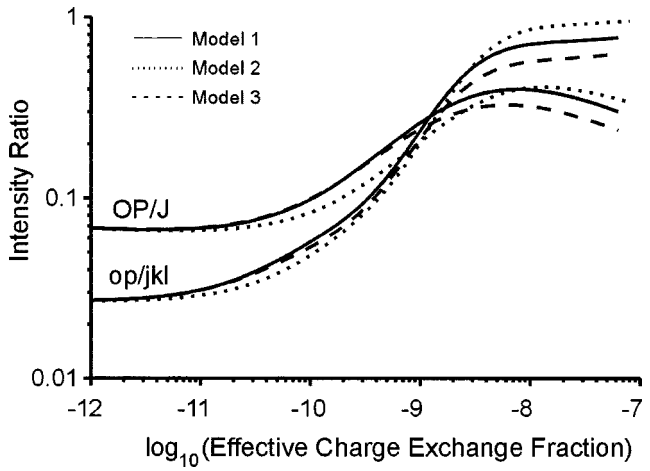

FIG. 10. Satellite-line intensity ratios $I(OP)/I(J)$ and $I(op)/I(jkl)$, calculated using different models (see text) for the determination of the populations of the $2\ell 2\ell'$ and $1s2\ell 2\ell'$ states, and adopting various models for the ℓ-state distributions (see text): parabolic projection (model 1), successive weak-field limit (model 2), statistical population (model 3), $V=10^8$ cm/s, $n_e=10^{22}$ cm^{-3}, $kT_e=700$ eV, and $L_{\text{eff}}=500$ μm.

We note that the results in Fig. 9 have been calculated for a silicon plasma with $kT_e=700$ eV, which is consistent with the measurement (see earlier details and the light gray plasma volume in Fig. 7). A sufficient density of donor ions (indicated by the dark gray area in Fig. 7) is, however, attained only for much lower temperatures. The results in Fig. 9 have therefore been obtained in a somewhat inconsistent manner: the hot-electron temperature (which determines the density of receptor ions n_i by means of the collisional-radiative model) has been kept fixed with a fixed value of the donor-ion density n_i^{donor}. In reality, the hot plasma (indicated by the light gray area in Fig. 7) can interpenetrate with the colder dense plasma. This situation, however, is entirely transient: hot plasma can mix with cold plasma undergoing charge-transfer processes and recombination cooling. The effective charge-transfer fraction f_x can therefore also be interpreted in such a manner that only a fraction of potential receptor ions undergo the charge-transfer process with the colder dense plasma (see the arrows in Fig. 7). The particular values obtained for the OP/J and op/j intensity ratios, which are presented in Fig. 9, are nevertheless representative due to the following reason: The stationary assumption of a fixed high temperature increases primarily the inner-shell excitation rates, because the charge-transfer rates tend to shift the ionic-level populations toward lower charge states. However, since the electron temperature is not lowered, inner-shell excitation rates are overestimated. Increased inner-shell excitation rates, however, do not appreciably affect the values predicted for the OP/J and op/j intensity ratios. This

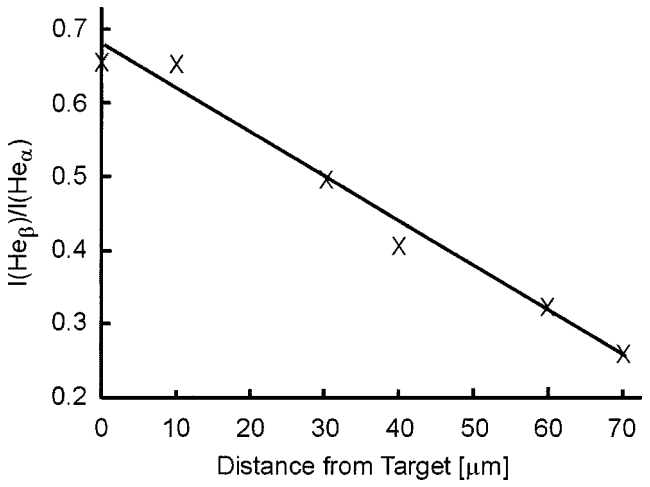

FIG. 11. Experimental line-intensity ratio $I(\mathrm{He}_\beta)/I(\mathrm{He}_\alpha)$ as a function of the target distance in the TRIDENT experiment. Far from the target, the ratio has its usual value, whereas close to the target, enhanced ratios are observed.

can be seen from the discussion of hot-electron effects presented above and in Fig. 6: the intensity ratios do not vary and, in particular, do not rise with increasing hot-electron fraction. Again, this indicates a minor influence of inner-shell excitation processes.

Figure 10 shows the influence on the line-intensity ratios of adopting various models for the ℓ distribution. It can be seen clearly that, in all cases considered, the principal parameter dependences are retained and that charge-exchange processes may lead to a considerable rise (by about a factor of 10) in the line-intensity ratios. The absolute values of the enhancement depend on the ℓ-distribution values W: for a larger population of the $2s^2$ levels, compared with that of the $2p^2\ {}^1D$ level, we find an increased line-intensity ratio.

D. He_β emission

Figure 11 shows a strong rise in the (relative) He_β emission with decreasing target distance in the TRIDENT experiments. The observed $\mathrm{He}_\beta/Ly_\alpha$ and $\mathrm{He}_\beta/\mathrm{He}_\alpha$ line-intensity ratios are found to be in agreement with our calculations, which are presented in Figs. 3–6, only at large distances from the target. In Fig. 8 we have presented the results obtained including charge-exchange processes, with cross section determined using Eq. (23). These results indicate that the $n=3$ states (which are the upper states in the He_β-line emission) may also be readily populated. For lower charge states of the donor ions, e.g., Be-through Ne-like ions, the preferentially populated states are $n \geqslant 3$. This leads to a strong charge-transfer produced population of the upper states in the He_β-line emission. This result is consistent with the observation of high He_β-line intensities near the target surface. In this connection, Fig. 9 shows a noteworthy variation of the various line-intensity ratios. For an effective charge-exchange fraction of about 10^{-8}, high op/j and OP/J intensity ratios are found together with high $\mathrm{He}_\beta/\mathrm{He}_\alpha$ and $\mathrm{He}_\beta/Ly_\alpha$ ratios, in agreement with the observations.

VI. CONCLUSIONS

Unusually enhanced emission, by an order of magnitude, of two-electron (dielectronic-satellite) transitions of He-like and Li-like ions in laser-produced plasmas has been investigated, both experimentally and theoretically. By means of a detailed collisional-radiative model for non-Maxwellian and partially optically thick plasmas, it has been shown that the observed discrepancies cannot be explained by taking into account only the usual collisional-radiative-model line-formation processes. These results are significant because dielectronic-satellite spectra are extensively used for diagnostics in numerous laser-plasma experiments. Large discrepancies would be detrimental for almost all interpretations. In the present work, we propose that ion-ion charge-transfer processes between highly charged silicon ions (moving in plasma jets near the target) and low-charged ions (near the surface) populate primarily excited states with low-lying quantum numbers. This is consistent with the observed satellite spectra. The existence of plasma jets is correlated with the observation of localized K_α emission produced by hot electrons impinging onto the target surface. The results obtained from our extended collisional-radiative model, which has been augmented to include charge-exchange processes, indicate that these additional processes can lead to enhanced emissions and significant modifications of the dielectronic-satellite spectra. At present, further improvements in the quantitative spectroscopic calculations should be possible with the availability of reliable results for the single-electron and double-electron charge-transfer cross sections relevant to ion-ion collisions. We anticipate that the present work will provide motivation for further spectroscopic measurements of the dielectronic-satellite emissions and new theoretical investigations of the relevant charge-transfer processes.

ACKNOWLEDGMENTS

This work was performed under the auspices of the ''Feodor-Lynen Nachkontaktprogramm'' of the Alexander von Humboldt Foundation (AvH) by two of us (F.B.R. and H.R.G.). The financial support of the AvH under Contract Nos. V-3-FLF-DEU1023793 and V-2-FLF-DEU1023793 is gratefully acknowledged. One of us (F.B.R.) also acknowledges the hospitality and support of the Institute for Plasma Research at the University of Maryland. Support at the University of Maryland of the National Science Foundation is acknowledged. The research work of V.L.J. was supported by the U.S. Department of Energy and by the Office of Naval Research.

[1] H. R. Griem, *Plasma Spectroscopy* (McGraw-Hill, New York, 1964).
[2] V. A. Boiko, A. V. Vinogradov, S. A. Pikuz, I. Yu. Skobelev, and A. Ya. Faenov, J. Sov. Laser Res. **6**, 82 (1985).
[3] H. R. Griem, Phys. Fluids B **4**, 2346 (1992).
[4] H. R. Griem, *Principles of Plasma Spectroscopy* (Cambridge University Press, New York, 1997).
[5] A. H. Gabriel, Mon. Not. R. Astron. Soc. **160**, 99 (1972).
[6] V. A. Vinogradov, I. Yu. Skobelev, and E. A. Yukov, Sov. Phys. JETP **45**, 925 (1977).
[7] V. L. Jacobs and M. Blaha, Phys. Rev. A **21**, 525 (1980).
[8] F. B. Rosmej and J. Aballah, Jr., Phys. Lett. A **245**, 548 (1998).
[9] F. B. Rosmej, A. Ya. Faenov, T. A. Pikuz, F. Flora, P. Di Lazzaro, T. Letardi, A. Grilli, A. Reale, L. Palladino, G. Tomassetti, and A. Scafati, J. Phys. B **31**, L921 (1998).
[10] A. Ya. Faenov, S. A. Pikuz, A. I. Erko, B. A. Bryunetkin, V. M. Dyakin, G. V. Ivanenkov, A. R. Mingaleev, T. A. Pikuz, V. M. Romanova, and T. A. Shelkovenko, Phys. Scr. **50**, 333 (1994).
[11] F. B. Rosmej, A. Ya. Faenov, T. A. Pikuz, F. Flora, P. Di Lazzaro, S. Bollanti, N. Lisi, T. Letardi, A. Reale, L. Palladino, D. Batani, A. Bornardinello, A. Scafati, L. Reale, A. Zigler, M. Fraenkel, and R. D. Cowan, J. Quant. Spectrosc. Radiat. Transf. **58**, 859 (1997).
[12] F. B. Rosmej, A. Ya. Faenov, T. A. Pikuz, I. Yu. Skobelev, A. E. Stepanov, A. N. Starostin, V. S. Rerikh, V. A. Magunov, F. Flora, S. Bollanti, P. Di Lazzaro, T. Letardi, K. Vigli-Papadaki, A. Grilli, L. Palladino, A. Reale, A. Scafati, and L. Reale, JETP Lett. **65**, 708 (1997).
[13] R. C. Elton, J. A. Cobble, H. R. Griem, D. S. Montgomery, R. C. Mancini, V. L. Jacobs, and E. Behar, J. Quant. Spectrosc. Radiat. Transf. **65**, 185 (2000).
[14] http://www-cxro.lbl.gov/optical_constants/
[15] B. L. Henke, J. Y. Uejio, G. F. Stone, C. H. Dittmore, and F. G. Fujiwara, J. Opt. Soc. Am. B **3**, 1540 (1986).
[16] B. L. Henke, P. Lee, T. J. Tanaka, R. L. Shimabukuro, and B. K. Fujikawa, At. Data Nucl. Data Tables **27**, 1 (1982).
[17] F. B. Rosmej, J. Phys. B **30**, L819 (1997).
[18] V. L. Jacobs and J. Davis, Phys. Rev. A **18**, 697 (1978).
[19] F. E. Irons, J. Quant. Spectrosc. Radiat. Transf. **22**, 1 (1979).
[20] G. Athay, *Radiation Transport in Spectral Lines* (Reidel, Dordrecht, 1972).
[21] G. D. Pollak, N. D. Delamater, J. K. Nash, and B. A. Hammel, J. Quant. Spectrosc. Radiat. Transf. **51**, 303 (1994).
[22] R. C. Mancini, R. F. Joyce, and C. F. Hooper, Jr., J. Phys. B **20**, 2975 (1987).
[23] R. L. Kelly, J. Phys. Chem. Ref. Data, Suppl. No. **16**, 1 (1987).
[24] R. D. Cowan, *Theory of Atomic Structure and Spectra* (University Press, Berkeley, 1981).
[25] L. A. Vainshtein and U. I. Safronova, At. Data Nucl. Data Tables **21**, 49 (1978).
[26] L. A. Vainshtein and U. I. Safronova, Phys. Scr. **31**, 519 (1985).
[27] V. P. Shevelko and L. A. Vainshtein, *Atomic Physics for Hot Plasmas* (IOP, Bristol, 1993).
[28] F. B. Rosmej, J. Phys. B **33**, L1 (2000).
[29] S. Kienle, F. B. Rosmej, and H. Schmidt, J. Phys. B **28**, 3675 (1995).
[30] F. B. Rosmej, Phys. Rev. E **58**, R32 (1998).
[31] V. N. Ostrovsky, J. Phys. B **28**, 3901 (1995).
[32] I. Yu. Tolstikhina and V. P. Shevelko, Short Commun. Phys. (Moscow) **5**, 46 (2000).
[33] R. K. Janev, L. P. Presnyakov, and V. P. Shevelko, *Physics of Highly Charged Ions* (Springer, Berlin, 1985).
[34] A. Müller and E. Salzborn, Phys. Lett. **62A**, 391 (1977).
[35] M. Lal, M. K. Srivastava, and A. N. Tripathi, Phys. Rev. A **26**, 305 (1982).
[36] J. Tharamel, V. A. Kharchenko, and A. Dalgarno, Phys. Rev. A **50**, 496 (1994).
[37] V. A. Abramov, V. S. Lisitsa, and A. Yu. Pigarov, JETP Lett. **42**, 356 (1985).
[38] M. I. Chibisov, Sov. Phys. JETP **70**, 1687 (1976).
[39] M. I. Chibisov, Sov. Phys. JETP **75**, 1222 (1978).